THE JOURNAL OF PHYSICAL CHEMISTRY B

Article

pubs.acs.org/JPCB

Differentiation of Rubidiated Methyl-D-Glycoside Stereoisomers by Infrared Multiple-Photon Dissociation Spectroscopy in the O−H and C−H Stretching Regions

Wright L. Pearson, III,[#,†] Cesar Contreras,[#,‡] David Powell,[#] Giel Berden,[&] Jos Oomens,[&,%] Brad Bendiak,[@] and John R. Eyler*[,#]

[#]Department of Chemistry, University of Florida, Gainesville, Florida 32611-7200, United States

[&]Radboud University, Institute for Molecules and Materials, FELIX Laboratory, Toernooiveld 7c, 6525 ED Nijmegen, The Netherlands

[%]University of Amsterdam, Science Park 904, 1098XH Amsterdam, The Netherlands

[@]Department of Cell and Developmental Biology and Program in Structural Biology and Biochemistry, University of Colorado Health Sciences Center, Denver, Colorado 80045, United States

Supporting Information

ABSTRACT: Four isomeric sugar methylglycosides (α- and β-D-gluco- and galactopyranosides) were evaluated as rubidium cation coordination adducts in the gas phase using variable-wavelength multiple-photon dissociation in the range from 2750 to 3750 cm^{-1}. The adducts dissociated following photon absorption to yield neutral sugars and the rubidium cation, resulting in infrared "action" spectra. Well-resolved hydroxyl stretching bands clearly differentiate stereoisomers that vary solely in their asymmetry at single carbons. Density functional theory calculations of the lowest-energy gas-phase complexes indicate that rubidium coordinates with lone pairs of oxygen atoms as either bi- or tridentate complexes and that more than one positional coordination isomer could adequately account for most of the O−H stretch frequencies observed for each methylglycoside.

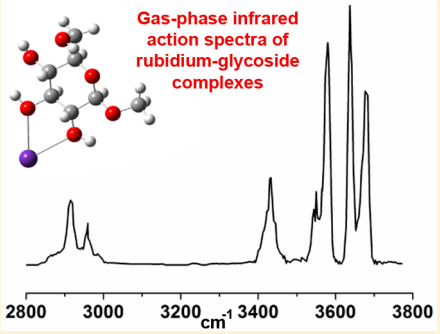

INTRODUCTION

Carbohydrates, the most abundant of biological molecules, provide important biological and economic functions, from energy storehouses in the human body and sweeteners in our beverages and foods, to cellulose for plant structure, and potential biofuels.[1,2] Many monosaccharides adopt a 6-membered cyclic structure. Much of the earlier work characterizing these compounds has been carried out in the solution phase.[2,3] Given the complexity of solution-phase chemistry, where carbohydrate derivatives and polymers have physical and spectral properties that vary with temperature, solvent, molecular structure, and so forth, gas-phase chemistry can be utilized to help simplify the picture.[4−6]

In particular, gas-phase experiments with charged proteins and other large biomolecules continue to increase our ability to study new areas of interest in chemistry and biology as mass spectrometric techniques evolve to allow more routine study of these large systems.[6−12] The techniques of Fourier transform ion cyclotron resonance mass spectrometry (FTICR-MS),[13−17] when combined with "soft" ionization techniques such as electrospray ionization (ESI),[10,18−20] allow the study of carbohydrate complexes without requiring heating of samples (thus inducing possible decomposition) in order to introduce them into the gas phase. Using FTICR-MS, ions derived from sugars can be studied at low pressures (below 10^{-9} Torr), providing a virtually collisionless environment to investigate basic chemical processes.

Collision-induced dissociation (CID)[21] and single-frequency infrared multiple-photon dissociation (IRMPD) methods have been used to study carbohydrate isomers in tandem MS experiments, both in positive and negative ion modes.[16,22−29] In some cases, when using either of these methods to examine isomeric compounds, particularly stereoisomers, differentiation of ions can be difficult as the two activation methods yield nearly identical dissociation patterns. Varying the wavelength of irradiation in IRMPD provides an extra dimension of analysis, since stereoisomers may not absorb photons identically over a range of wavelengths.[30−32] Recent studies using FTICR or ion trap mass spectrometers in conjunction with variable-wavelength IRMPD have shed new light on the structures of carbohydrates.[33−41] In addition, gas-phase techniques that have investigated neutral sugar molecules include molecular beam experiments with supersonic expansions[42] and microwave spectroscopy,[43,44] which have yielded detailed information about the structures of sugars without solvent or as single water molecule complexes.

Received: July 8, 2015
Revised: September 11, 2015
Published: September 22, 2015

DOI: 10.1021/acs.jpcb.5b06563
J. Phys. Chem. B 2015, 119, 12970−12981

Carbohydrates, even simple monosaccharides, can assume multiple configurations and/or conformations, sometimes favoring one over another depending on environmental influences such as interaction with metals, different solvents, and intramolecular hydrogen bonding.[45−48] A number of physical techniques, including NMR,[46] crystallography,[49] electrophoresis,[50,51] mass spectrometry, and theoretical calculations,[52,53] have focused on the interactions of sugars with metal ions. The conformation of glycans affects their role as components of larger biomolecules; they are important in cell−cell signaling[54] and have been found to affect protein folding in glycoproteins,[55] often stabilizing the protein structure.

To obtain a more complete picture of the role of oligosaccharides in protein-based systems, the interactions between alkali metals and sugars need to be understood in greater detail. Sodium and potassium play a crucial role in regulating cell functions, and their blood concentration levels are regulated in biological systems. Lithium ions are used as strong prescription drugs to regulate mood. Practically, alkali metals readily adduct with sugars, and such charged adducts can be transferred to the gas phase using electrospray ionization. This provides adequate abundances of precursor ions required to conduct reliable MS/MS experiments. If the alkali cation−sugar interaction is strong, fragmentation pathways other than simple cation loss may be favored when ions are subjected to irradiation with an infrared laser or CID. Intramolecular fragmentation is usually observed for Li^+-complexed saccharides.[22,56] However, potassium-, rubidium-, and cesium-complexed ions typically dissociate readily to yield only the alkali cation without fragmenting the saccharide. Of these, rubidium leads to the best-resolved IRMPD action spectra involving loss of the rubidium ion and was the choice for the experiments reported here.

Earlier IRMPD spectra obtained by Valle et al.[33] explored the infrared range from 600−1700 cm^{-1} to examine vibrational characteristics of the rubidium-glycoside isomers (Supporting Information). Only a few differentiable characteristics of the spectra were found among the different sugar isomers, due in part to the congested vibrational "fingerprint" region. However, peaks in the relatively isolated O−H stretching region (~3200−3700 cm^{-1}), produced by vibrations of the four hydroxyl groups in these ions, were thought to have a greater potential for monosaccharide structure differentiation, based on observations in molecular beam experiments.[42] With interest in the potential use of the hydroxyl stretch region for isomer-selective photodissociation in mass spectrometric analyses of sugars, herein we report theoretical ion structure/energetics calculations in combination with IRMPD spectra. Tunable optical parametric oscillator (OPO) lasers were used to probe the configuration of four rubidium-complexed glycosides. It is shown that this spectral region provides far more resolved spectral "fingerprints" that clearly differentiate ions having stereochemical differences at single asymmetric carbons of sugar molecules.

EXPERIMENTAL METHODS

A majority of the experiments were carried out at the University of Florida (UF). However, several confirmatory IRMPD spectra were obtained at the Free Electron Laser for Infrared eXperiments (FELIX) Laboratory in The Netherlands. Details of experiments performed at each location are discussed separately below.

Reagents and Materials. Structures of the four methyl-D-glycoside isomers are shown in Figure 1, and each has a molecular weight of 194 Da. Methyl glycosides were purchased from Sigma-Aldrich and were chosen to avoid the presence of different anomeric and ring forms (α and β furanose or pyranose) that occur in solution with the free sugars; thus, the molecules were locked as their single cyclic acetal configurations. Methanol (MeOH) and rubidium chloride were purchased from Sigma-Aldrich, and Milli-Q water (H_2O) was acquired from the physical chemistry teaching laboratory at the University of Florida. Stock solutions were prepared by dissolving 10 mg of each methyl glycoside in four separate 10 mL solutions of 80:20 MeOH:H_2O. Samples were taken as needed and diluted to 1×10^{-4} M at the same solvent ratio. Rubidium chloride (cationizing agent) was then added to the solutions in an amount sufficient to produce the same concentration (1×10^{-4} M) as that of the monosaccharides.

In experiments at the FELIX Laboratory, rubidium chloride, HPLC grade water, and methanol were all purchased from Sigma-Aldrich. Solutions for electrospray ionization were prepared with equimolar amounts of rubidium chloride and the O-methylated glycosides at a concentration of 1×10^{-3} M in 80:20 MeOH:H_2O.

Instrumentation. A tunable continuous-wave optical parametric oscillator (OPO) laser (LINOS Photonics OS 4000, Munich, Germany) aligned to the cell of a 4.7 T Bruker Apex II FTICR mass spectrometer (Bruker, Billerica, MA) with an Analytica electrospray (ESI) source (Analytica of Branford, Inc., Branford, CT), was employed for experiments at UF. Electrospray ionization at a flow rate of 2 μL/min was assisted by nebulizer and desolvation gas (N_2) at rates of 35 and 155 L/h, respectively. A 3.6 kV potential difference was applied between the ESI needle and capillary. Parent ions (rubidium-complexed glycosides) were isolated using swept frequency ejection pulses and irradiated. The products (depleted parent and rubidium ions) were detected in a 70−500 m/z window by broadband detection. A Bruker Xmass data acquisition system 7.0 was used to set instrument parameters and for data collection. A SYNRAD Series 48 CO_2 laser (Mukilteo, WA) with output wavelength of 10.63 μm was used as an off resonance source of IR photons to aid the OPO irradiation when necessary (as described below).

All ESI-FTICR-MS experiments at the FELIX Laboratory were carried out using an OPO laser (LaserVision, Bellevue WA, U.S.A.) aligned to the cell of a laboratory-built FTICR mass spectrometer equipped with a 4.7 T superconducting magnet (Cryomagnetics Inc., Oak Ridge, TN), which has been described previously.[33,57,58] An external Z-spray source (Micromass/Waters Corporation, Milford, MA) injected the samples into the ESI source at a flow rate of 10 μL/min. Electrospray ionization efficiency was aided with a nebulizer and a desolvation gas, both N_2. Source temperature was set to 45 °C, and the desolvation gas temperature was 100 °C. The electrospray needle-sampling cone voltage difference was set to 3 kV. Precursor ions were isolated using stored waveform inverse Fourier transform (SWIFT) waveforms[59,60] to eject all other ions. Ions were detected using the broadband detection mode.

Optical Parametric Oscillator Lasers. The tunable cw-OPO laser[61,62] used in experiments at UF differs somewhat from the pulsed OPO lasers used by several other groups[63−67] and for experiments at the FELIX Laboratory.[68−70] Its salient operating features are briefly described here. Electromagnetic

DOI: 10.1021/acs.jpcb.5b06563
J. Phys. Chem. B 2015, 119, 12970−12981

radiation from the continuous-wave pump laser (Nd:YAG), operating at 2W and a fixed wavelength of 1.064 μm (9398 cm^{-1}), interacted with a periodically poled lithium niobate (PPLN) crystal in one of 18 poling periods, to produce two different frequencies, the signal and idler, related as shown in eq 1.

$$\nu_p = \nu_s + \nu_i \quad (1)$$

where ν_p, ν_s, and ν_i are the frequencies of the pump, signal, and idler, respectively. A gradual rise/drop in temperature over the range 50−150 °C correspondingly moved the signal wavelengths up/down and the idler wavelengths down/up the poling period's wavelength range. This process brought consecutive groups of wavelengths into resonance with the cavity as the previous wavelengths were no longer in resonance. Wavelength discrimination was further enhanced by the inclusion of an etalon in the resonance cavity. After the acquisition of data for a given poling period, the temperature was reduced, and the position of the crystal was changed to an adjacent poling period to access the next series of wavelengths. The 18 poling periods available to the OS 4000 OPO laser covered wavenumber ranges of 7246−5000 and 4405−2141 cm^{-1} for signal and idler, respectively. The idler wavelength range (2270−4670 nm/4405−2141 cm^{-1}) and power (50−150 mW) were sufficient to allow the IRMPD spectra of the C−H (with the assistance of a CO_2 laser as explained later) and O−H stretches for the four complexes to be obtained.

It was experimentally most convenient to monitor the wavelength of the signal beam emitted by the OPO laser with a wavemeter (Model WA-1000, EXFO Inc. Quebec, Canada). The wavelength of the idler beam used for ion irradiation was calculated from the measured signal beam wavelength through substitution and rearrangement of the conservation of energy relationship eq 1. The OPO laser and much of its beam path were contained in a dry nitrogen purge box to reduce (also see below) absorption by gaseous water molecules in the laboratory environment.

The OPO at the FELIX Laboratory was a pulsed system producing 6 ns pulses with energies up to 20 mJ in the 2500−4000 cm^{-1} frequency range and with a bandwidth of 3.5 cm^{-1} at a repetition rate of 10 Hz. The system was pumped by a 600 mJ Nd:YAG-pumped laser (Innolas Spitlight 600) and consisted of an optical parametric oscillator with a single KTP (potassium titanyl phosphate) crystal pumped at a wavelength of 532 nm, as well as an optical parametric amplifier with four KTA (potassium titanyl arsenate) crystals pumped at a wavelength of 1064 nm. Wavelength tuning was achieved by angle-tuning the five crystals. Both the infrared laser and the beam path into the mass spectrometer were purged with dry nitrogen to prevent absorption of infrared laser light by atmospheric water and CO_2. Wavelength calibration was performed by recording the absorption lines of atmospheric water (before flushing with nitrogen) and by monitoring the near-infrared light of the signal beam around 780 nm in the OPO stage with a wavemeter (HighFinesse WS5).

EXPERIMENTAL PROCEDURE

For experiments at UF, after preparing a solution of one of the four Rb^+-[O-methyl- glycoside] complexes, the ions were introduced to the FTICR mass spectrometer via electrospray ionization, accumulated in a hexapole ion-trapping region for 1s, and transferred to the cell through a series of ion optics. Once trapped in the cell, the Rb^+ methyl-glycoside precursor ions (having m/z 279/281) were isolated and irradiated by the OPO idler beam at a set wavelength for 10s (for O−H stretches). Ten ion transient response signals were collected, averaged, and then subjected to Fourier transformation to obtain a mass spectrum. The relative abundances of the precursor and product ($^{85}Rb^+$ and $^{87}Rb^+$) ions were recorded. Subsequently, the OPO laser was adjusted for the next wavelength and the process was repeated (for wavenumbers ranging from 2750 to 3750 cm^{-1}). Mass spectra consisted of either the Rb^+-[O-methylated-glycoside] precursor ions with no dissociation products (nonresonant wavenumbers) or the depleted precursor ions with the Rb^+ dissociation products (resonant wavenumbers). The action spectrum was then plotted as the power-corrected natural logarithm of the $(P + F)/P$ ratio versus $\bar{\nu}$, where F corresponds to the combined relative abundance of $^{85}Rb^+$ and $^{87}Rb^+$ ions (the fragments) and P the relative abundance of the depleted precursor ions; the relative abundances of parent peaks containing both rubidium isotopes were summed.

At the University of Florida, rubidium ions were readily dissociated by resonant absorption of OPO infrared photons in the O−H stretch region (cw OPO power in the range 100−140 mW). However, relatively weak absorption at the C−H stretching frequencies generated small or no abundance for rubidium ion peaks under the same conditions. Fluence assistance to the ions resonantly excited by the OPO laser (in the quasicontinuum) was provided by off-resonant photons from the CO_2 laser when examining C−H stretch frequencies. The off-resonance condition was assured by past action spectra (Figure SI-1, Supporting Information), which illustrated a relatively featureless absorption region at the wavelength of the CO_2 laser of 10.6 μm. Blackbody and/or off-resonant effects were minimized by changing the power of the CO_2 laser and its irradiation time until a product ion-free spectrum was achieved when using only the CO_2 laser over the total irradiation period.

After trying several combinations of OPO and CO_2 laser irradiation times, it was found that a total OPO irradiation time of 15 s, with the CO_2 laser operating concurrently for the last 7 s produced sufficient fragmentation, where the CO_2 laser itself was subthreshold for dissociation events. For these experiments involving the C−H stretch region the power of the cw OPO laser was ∼40−60 mW with CO_2 laser powers in the range 150−200 mW. A greater extent of dissociation was achieved, with wavelength dependence, using off-resonance CO_2 laser preheating of the ion (Figure SI-2).

For experiments in both the O−H and C−H stretch regions, two to four mass spectra were obtained at approximately the same wavelength, often on different days. Points in the experimental IRMPD spectra discussed below for each of the four Rb^+-[O-methylated-glycoside] complexes were obtained by averaging all results in 2 cm^{-1} wavenumber intervals.

The different OPO laser system at the FELIX Laboratory necessitated a slightly different experimental procedure. Once trapped in the FTICR cell, the precursor ions were irradiated for 3 s with 30 pulses of the OPO laser. An infrared spectrum was obtained by plotting the natural logarithm of the $(P + F)/P$ ratio obtained from 3 summed mass spectra, as a function of infrared frequency (with 3 cm^{-1} steps).

COMPUTATIONAL DETAILS

Computational studies were carried out with Gaussian 09 utilizing density functional theory (DFT) with the B3LYP

DOI: 10.1021/acs.jpcb.5b06563
J. Phys. Chem. B 2015, 119, 12970−12981

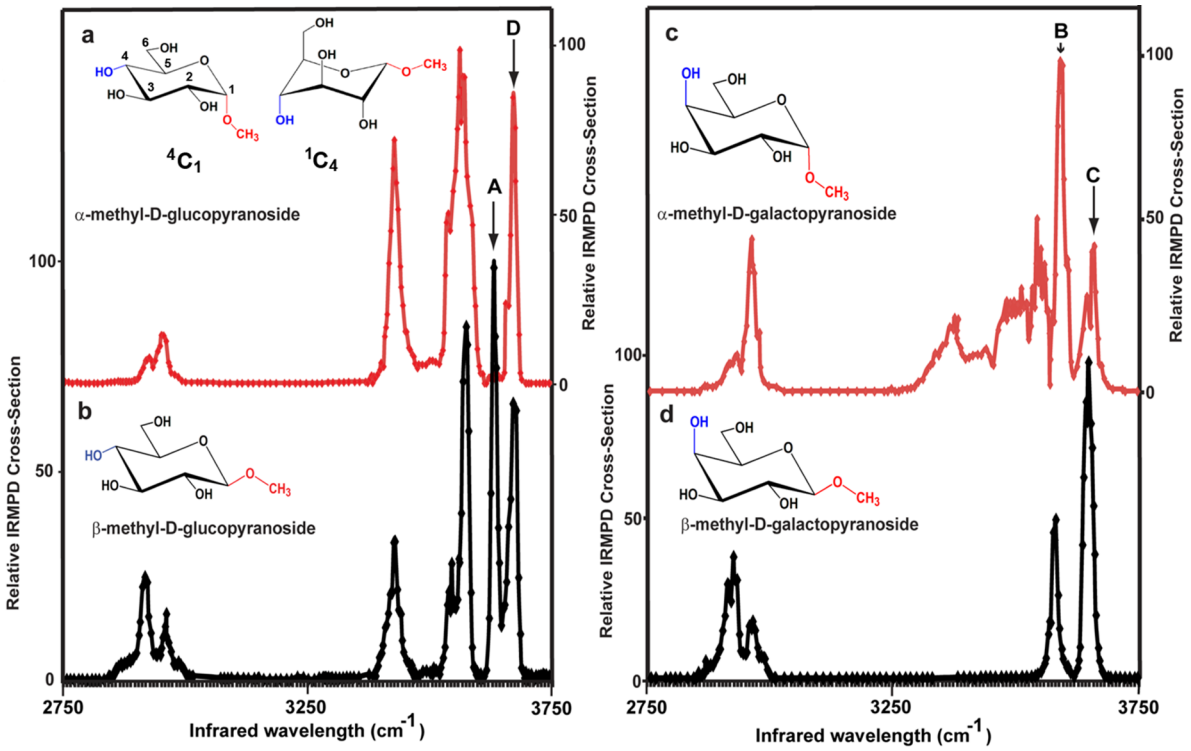

Figure 1. Experimental gas-phase infrared multiple-photon dissociation spectra and structures of four methylglycosides as Rb^+ coordination adducts, in the spectral range from 2750 to 3750 cm^{-1}. Shown are spectra of (a) α-methyl-D-glucopyranoside, (b) β-methyl-D-glucopyranoside, (c) α-methyl-D-galactopyranoside, (d) β-methyl-D-galactopyranoside. Arrows indicate spectral features discussed in the text. The two chair conformations ($^4C_1$ and $^1C_4$) are defined, and sugar ring carbons are labeled as indicated in panel a.

hybrid functional and 6-31+G (d) and (for Rb^+) Stuttgart-Dresden (SDD) basis sets.[71] Geometrically optimized $^4C_1$,$^1C_4$, and boat configurations for each sugar were first constructed. Each of these structures was in turn placed in a three-dimensional grid for consistent Rb^+ attachment spacing. A single rubidium ion was carefully positioned above, around, and below each carbon atom, the oxygen atom in the ring, and the bonds connecting these atoms, as well as above and below the hexose ring and its interior and the configuration saved after each placement. Rotation of the hydroxyl group about the bond between C-5 and C-6 was also considered for greater model flexibility. Geometric optimizations and vibrational frequencies were computed. The Gabedit[72] program was used to generate infrared spectra—predicted peaks were convoluted with a Gaussian line shape (5 cm^{-1} half-width) and a frequency scaling factor of 0.957 was used for the O−H stretch region—and to convert the theoretical spectra into x-y coordinates for evaluation of all conformers with experimental spectra using Excel. Zero point energies were also recorded with the lowest energy structures noted for comparison.

RESULTS AND DISCUSSION

Infrared multiple-photon dissociation spectra in the wavenumber region from 2750 to 3750 cm^{-1} and structures of the four Rb^+-[O-methyl-glycosides] are shown in Figure 1 (all measured at UF).

Experimental spectra generally exhibited two to four distinct peaks in the O−H stretch region, and two or more peaks in the C−H stretch region. It is worthy of note that the O−H stretch region generally showed much better resolution and differentiation between stereoisomers as compared to our earlier studies[35,73] of various sugars in the spectral region from 700 to 1800 cm^{-1} (see also Figure SI-1). Similar observations of well-resolved hydroxyl stretch frequencies have been observed for neutral gas-phase sugar molecules in molecular beam experiments.[42]

Each methyl glycoside yields a unique spectrum that clearly differentiates it; sets of structures were compared that vary solely in the stereochemistry at a single carbon, which includes spectral comparisons between C-1 anomers and C-4 epimers. For spectra of the α- and β-methyl glucosides (panels a and b, Figure 1), a comparison revealed a peak at 3637 cm^{-1} (arrow A) that was observed for the β but not the α anomer. Similarly, in comparing spectra of the α- and β-methyl galactosides (panels c and d, Figure 1), only two major peaks centered at 3582 and 3649 cm^{-1} were observed for the β anomer. In the α anomer, two narrow peaks are observed at 3592 and 3662 cm^{-1} (arrows B and C, Figure 1c) that are clearly blue-shifted from those of the β-anomer (Figure 1d). Additionally, the α anomer shows a complex absorption in the range from about 3300 to 3570 cm^{-1}. Furthermore, in comparing the methylglucosides with the methylgalactosides, a characteristic peak at 3677 cm^{-1} (Figure 1a and b, arrow D) was observed that distinguishes both methylglucosides from their 4-epimeric counterparts (the methylgalactosides, Figure 1c and d), in addition to other unique differences that clearly distinguish single sets of the 4-epimers (compare Figure 1a with c and Figure 1b with d). Overall, the data indicate that photodissociation experiments in the hydroxyl stretch region are very useful for high-resolution discrimination between sugar stereoisomers. Moreover, the spectra of Figure 1 are far better resolved than condensed phase spectra, where this spectral region generally shows a broad single overlapped peak due to intermolecular and/or solvent interactions.[74]

DOI: 10.1021/acs.jpcb.5b06563
J. Phys. Chem. B 2015, 119, 12970−12981

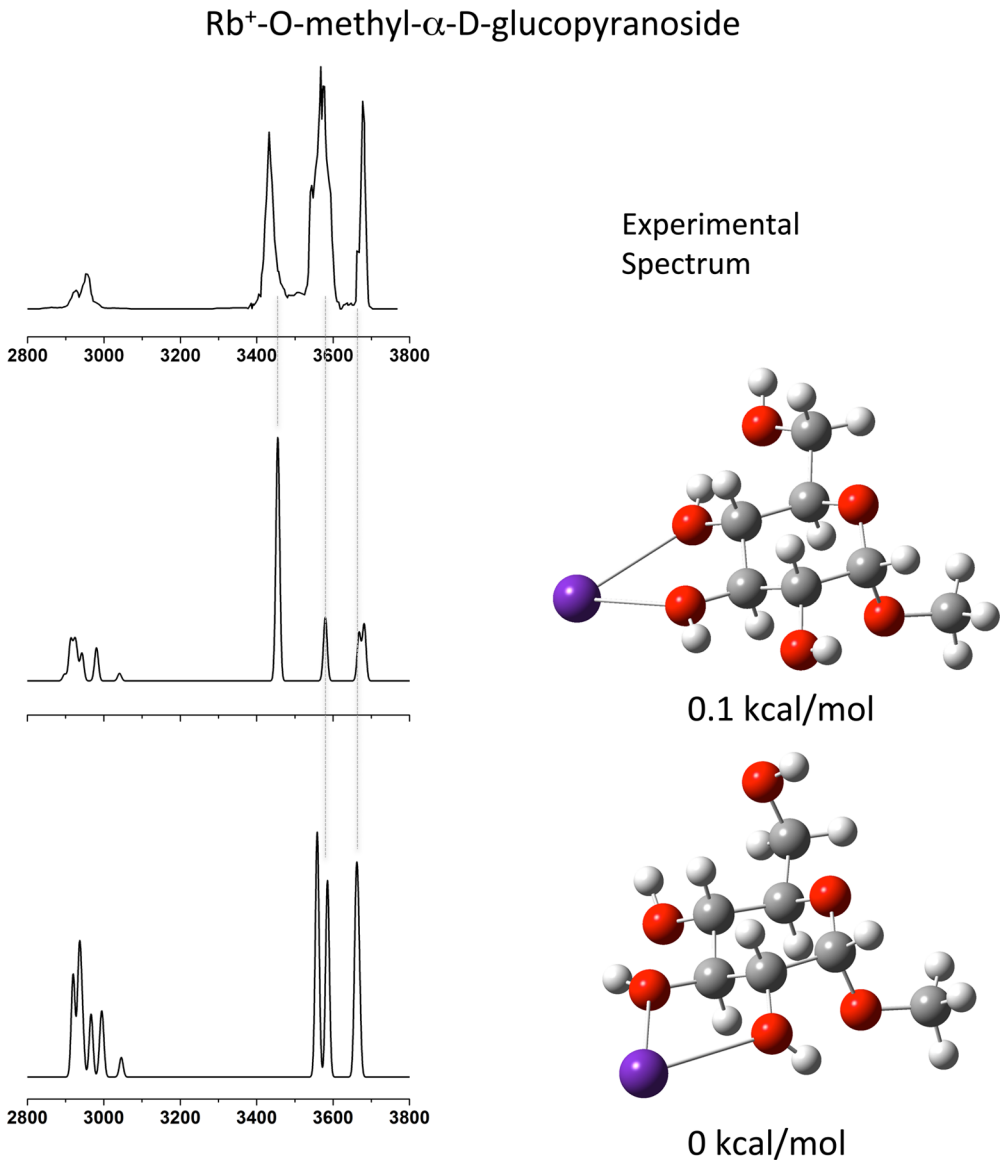

Figure 2. Calculated spectra, relative energies, and structures of two different coordination complexes of Rb^+-*O*-methyl-*α*-D-glucopyranoside (lower two panels) compared to the experimental spectrum (upper panel). The structure in the middle is the 3,4-OH−Rb^+ coordination complex, and the structure at the bottom is the 2,3-OH−Rb^+ coordination complex.

It is also worth pointing out that experimental differences were observed in the C−H stretch region (about 2840−3000 cm^{-1}) for all four glycosides. While obvious, these differences were less discriminatory. Ten different C−H stretching frequencies contribute to the overlapping peaks seen in the C−H stretch region and the infrared intensities of the peaks in this region were also relatively weak. Each of the four glycosides will be discussed in greater detail in turn below, and the calculated lower energy structures with predicted O−H stretching bands corresponding to those seen in the experimental spectra will be presented.

GLUCOSIDES

***O*-Methyl-*α*-D-Glucopyranoside (*α*Glc).** The experimental spectrum for this glycoside is shown in Figure 2, together with the calculated spectra, relative energies, and structures of two theoretically calculated low-energy coordination isomers. The two isomers are calculated to be very close in energy, so that both are probably present under the conditions of these experiments. The theoretically calculated positions of their O−H stretching bands adequately explain the experimentally observed spectrum in the O−H stretch region, as a summed combination of both isomeric species.

The calculated lowest energy isomer, shown in the bottom panel of Figure 2, has a $^4C_1$ conformation. The O−H stretching frequencies for OH4 and OH6 are very similar, resulting in a predicted peak at ∼3664 cm^{-1}. As seen in the figure, the Rb^+ cation is predicted to be bound to the oxygen lone pairs of OH2 and OH3, thus red-shifting their O−H stretching frequencies respectively to ∼3558 and 3584 cm^{-1}.

The second low-energy isomer, shown in the middle panel of Figure 2, also has a $^4C_1$ conformation and the predicted O−H stretching frequencies for OH6 (3682 cm^{-1}) and OH2 (3667 cm^{-1}) combine to produce the slightly split peak in that wavenumber range seen in the figure. As with the lowest energy isomer, the O−H stretching frequencies for the two hydroxyl groups bound to Rb^+, OH3, and OH4 in this isomer are predicted to be red-shifted. The hydrogen atom of OH4 is

DOI: 10.1021/acs.jpcb.5b06563
J. Phys. Chem. B 2015, 119, 12970−12981

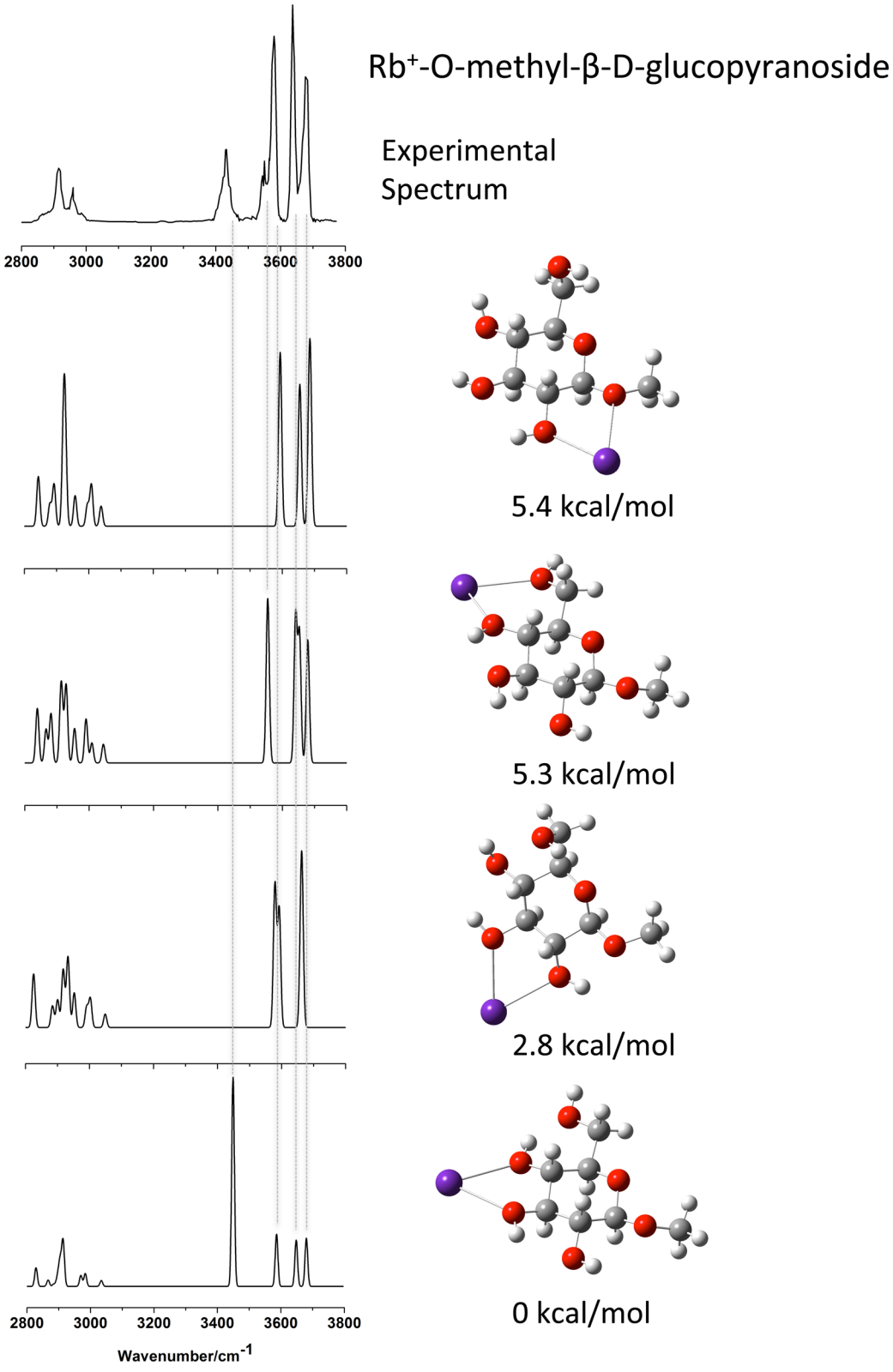

Figure 3. Theory-predicted spectra, relative energies, and structures for four different coordination complexes of lowest energies (lower four panels) and experimental spectrum (upper panel) of Rb^+-*O*-methyl-*β*-D-glucopyranoside. Shown, from the bottom up, are the 3,4-OH; 2,3-OH; 4,6-OH; and 1OMe, 2OH-Rb^+ coordination complexes.

hydrogen bonded to the oxygen atom of OH6, and the distance between these two atoms is calculated to be 1.84 Å, considerably shorter than any other O···H hydrogen bonding distance in either of the two calculated lowest energy isomers (e.g., the distance between the H atom in OH3 and the O atom in OH4 is calculated as 2.24 Å for the lowest energy structure). This relatively short hydrogen bonding distance results in a predicted further red shift of the O−H stretching frequency of

DOI: 10.1021/acs.jpcb.5b06563
J. Phys. Chem. B 2015, 119, 12970−12981

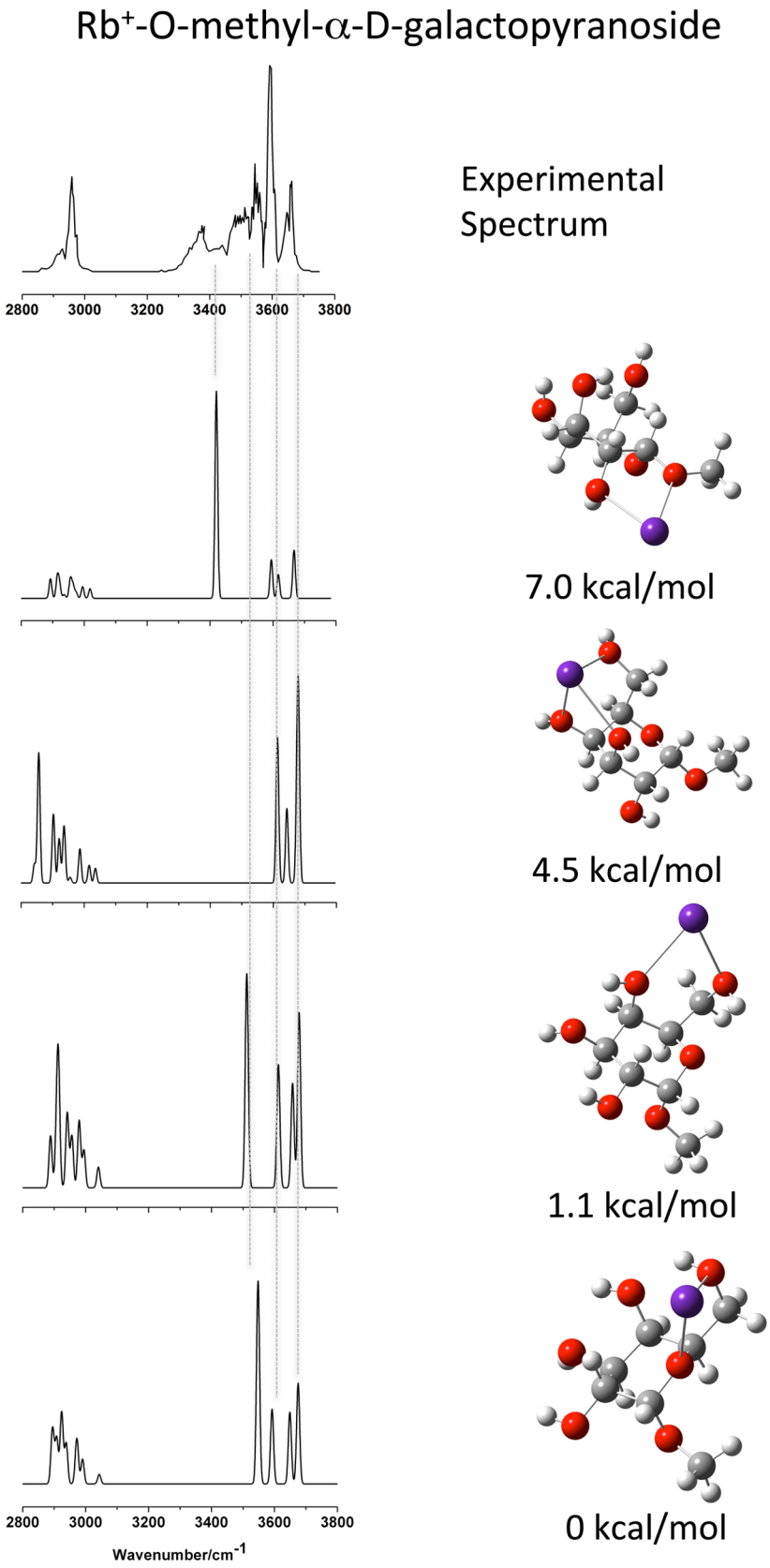

Figure 4. Theoretical spectra, relative energies, and structures for four low energy coordination isomers (lower four panels) and experimental spectrum (upper panel) of Rb^+-*O*-methyl-*α*-D-galactopyranoside. Shown, from the bottom up, are the OH6, ring O, 4,6-OH, 3,4,6-OH, and 1OMe, 2OH-Rb^+ coordination complexes.

OH4, leading to the peak seen at ∼3455 cm^{-1} in the middle spectrum in Figure 2.

***O*-Methyl-*β*-D-Glucopyranoside (*β*Glc).** The IRMPD spectrum of Rb^+-*O*-methyl-*β*-D-glucopyranoside is shown in

DOI: 10.1021/acs.jpcb.5b06563
J. Phys. Chem. B 2015, 119, 12970−12981

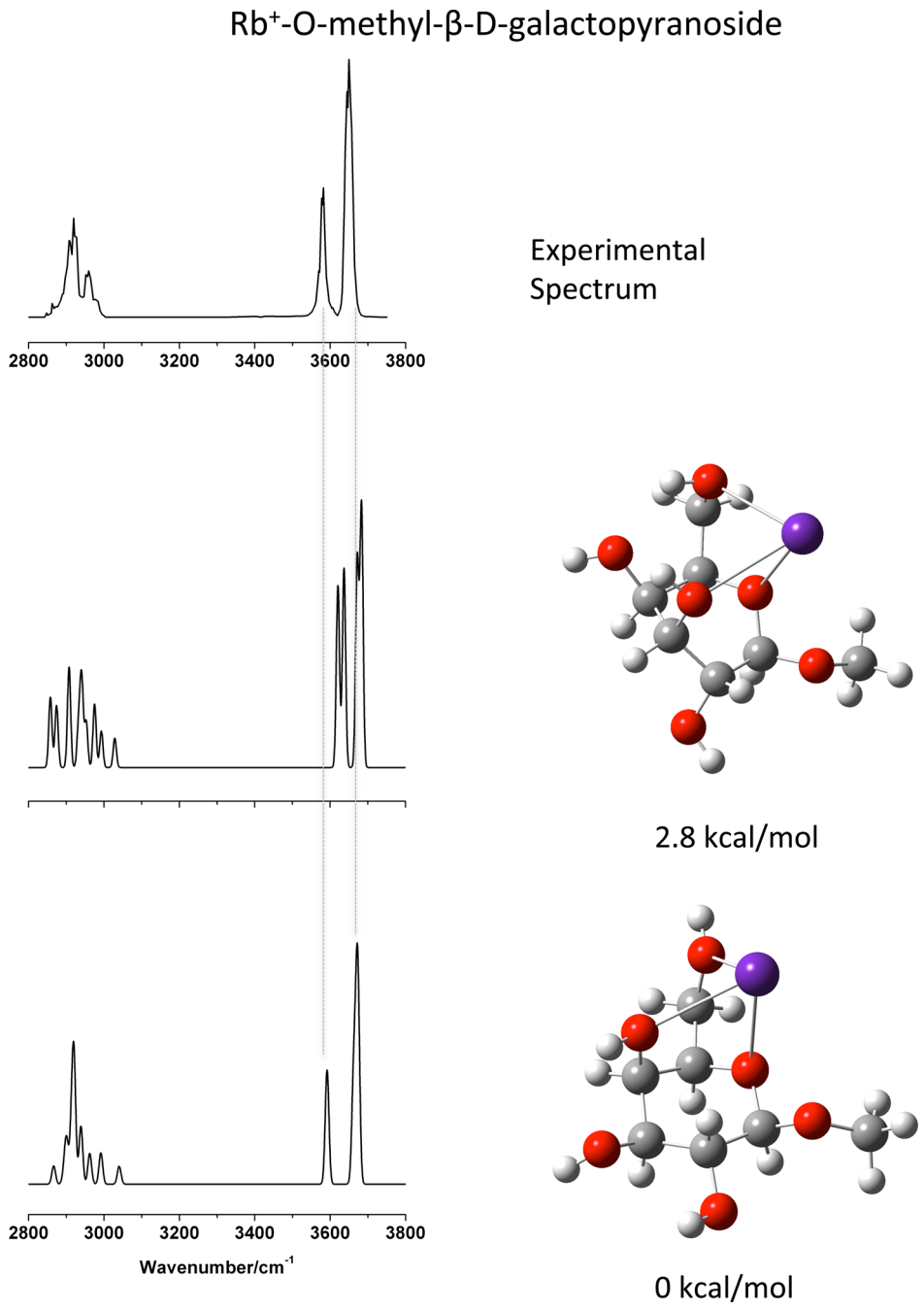

Figure 5. Calculated spectra, relative energies, and structures (lower two panels) and experimental spectrum (upper panel) of Rb^+-*O*-methyl-*β*-D-galactopyranoside. The lowest energy form is an OH4, OH6, ring O tridentate coordinated structure, whereas the higher energy form is an OH3, OH6, ring O tridentate coordinated structure having a skewed conformation.

the top panel of Figure 3 with the spectra and structures of four bidentate coordination isomers shown below it. These structures were calculated to be among the lowest in energy, all having $^4C_1$ conformations.

For each of the four calculated structures, as was discussed above for Rb^+-*O*-methyl-*α*-D-glucopyranoside, the most red-shifted O−H stretching bands are those for hydroxyl groups to which the rubidium cation is bound. The calculated lowest energy structure contained a bidentate coordination of Rb^+ with hydroxyl groups 3 and 4 (bottom of Figure 3) and, with its predicted red-shifted OH stretching peak at 3449 cm^{-1}, is very similar to that shown in the middle of Figure 2, except for the inversion of configuration at C1. As with the Rb^+-*O*-methyl-*α*-D-glucopyranoside structure, the red-shifted peak of the lowest energy Rb^+-*O*-methyl-*β*-D-glucopyranoside conformer corresponds to an OH4 stretch, shifted by bonding to the Rb+ cation and a predicted very short (1.84 Å) hydrogen bonding distance between the H atom of OH4 and the O atom of OH6.

Interestingly, the least red-shifted band for the third highest energy conformer (middle spectrum of Figure 3) corresponds to the stretching frequency of OH6, to which Rb^+ is predicted to be bound. As can be seen in the figure, OH6 is not hydrogen bonded to any of the other hydroxyl groups in the ion. Apparently the red-shifting effect of binding from a rubidium ion calculated to be 2.84 Å from the O atom in OH6 is not as great as, for example, hydrogen bonding from two hydroxyl

DOI: 10.1021/acs.jpcb.5b06563
J. Phys. Chem. B 2015, 119, 12970−12981

groups to OH3 whose O atom is 2.15 Å from the H atom in OH4 and whose H atom is 2.51 Å from the O atom in OH2, which results in the most red-shifted peak observed for the structure in the middle spectrum of Figure 3. Other bidendate structures having a Rb^+ coordinated with the 2- and 3-OH oxygens, or the 2-OH and anomeric O-Me oxygens, also yielded calculated frequencies compatible with those of the experimental spectrum (Figure 3).

GALACTOSIDES

***O*-Methyl-α-D-Galactopyranoside (αGal).** Figure 4 (top) shows the experimental spectrum for this rubidiated sugar molecule, with the spectra, relative energies, and structures of four DFT calculated low energy forms shown in the lower panels.

The two lower energy structures in Figure 4 have a $^4C_1$ conformation, and the O−H stretch peak that is most red-shifted is predicted to be associated with a hydroxyl group to which Rb^+ is bound (OH6 and OH4 for the lowest and second lowest energy structures in Figure 4, respectively). The rubidium ion is predicted to be bound to the sugar ring oxygen atom in the lowest energy structure, but in the second lowest energy structure shown, it is predicted to be bound to the oxygen atoms of two hydroxyl groups, OH6 and OH4, and the second most red-shifted band, at ∼3610 cm^{-1}, is associated with OH6.

The two higher energy structures in Figure 4 have a $^1C_4$ conformation. In the second highest energy structure, the most red-shifted O−H stretch peak corresponds to OH2, whose H atom is hydrogen bonded to the methoxy oxygen. Apparently, the red-shifting effect of Rb^+ cation bonding to the oxygen atoms of OH3, OH4, and OH6 is lessened due to its coordination to three OH groups. In the highest energy structure shown, the significantly red-shifted peak corresponds to the OH3 stretching frequency. The $^1C_4$ conformation of this structure allows the OH3, OH4, and OH6 groups to form a strong hydrogen-bonding network, with the hydrogen of OH4 bonded to the oxygen of OH3, and the hydrogen of OH3 bonded to the oxygen of OH6.

***O*-Methyl-β-D-Galactopyranoside (βGal).** The experimental spectrum for this anomer is shown at the top of Figure 5, with the spectra, relative energies and structures of two calculated low-energy conformers shown in the lower panels of the figure.

As can be seen in Figure 5, the spectrum of the calculated lowest energy structure matches the experimental spectrum quite well. For that structure ($^4C_1$ conformation), the rubidium ion is predicted to be above the sugar ring and bound not only to two hydroxyl groups (OH4 and OH6) but also to the ring oxygen atom (a tridentate complex). In the higher energy structure, the rubidium ion is also predicted to be tridentate and bound to two hydroxyl groups (OH3 and OH6) and the ring oxygen atom. The sugar ring in this structure has a skewed conformation.

The O−H stretching band associated with OH4 is predicted to be most red-shifted in the lowest energy structure (3592 cm^{-1}), due to bonding with Rb^+ and hydrogen bonding of its hydrogen atom with the oxygen atom of OH3. The effects of Rb^+ and/or hydrogen bonding are apparently quite similar for the other three hydroxyl groups, as the O−H stretching frequencies are predicted to be virtually identical (3675 cm^{-1} for OH6, 3670 cm^{-1} for OH3, and 3661 cm^{-1} for OH2) and, with the spectral resolution used to generate the spectrum, give rise to a single band.

The calculated spectrum for the higher energy (skewed) structure does not appear to match quite as well with that found experimentally. Given that its energy is predicted to be 2.8 kcal/mol higher than that of the lowest energy structure, it should be populated to some extent in our experiments. Its two least red-shifted bands at 3683 cm^{-1} (OH4 stretch) and 3672 cm^{-1} (OH2 stretch) may combine with the lower energy structure's band at ∼3670 cm^{-1} to produce the slightly broadened peak seen in the experimental spectrum. The two more red-shifted bands at 3637 cm^{-1} (OH3 stretch) and 3620 cm^{-1} (OH6 stretch) do not match the most red-shifted band in the experimental spectrum (3582 cm^{-1}) as well as the predicted band at 3592 cm^{-1} for the lowest energy structure.

Spectral Reproducibility: Comparison of Spectra Obtained in Two Laboratories. Application of the IRMPD technique in ion spectroscopy is relatively new. Line broadening and line intensities resulting from the multiple-photon excitation process are often the subject of discussion.[75] From an experimental point of view, interinstrument comparisons are a necessary and important evaluation of such a novel method, but these comparisons are, however, very scarce[76,77] given the variety of mass spectrometers (ion trap, FTICR, etc.) and infrared light sources (free electron lasers, cw- and pulsed-OPOs, etc.) used to obtain IRMPD spectra.

Experimental IRMPD spectra for Rb^+-*O*-methyl-α-D-glucopyranoside were obtained at both UF and the FELIX Laboratory, and a comparison of the O−H stretch region in the two spectra is shown in Figure 6. Excellent agreement can be seen for both the frequencies and the intensities of bands for

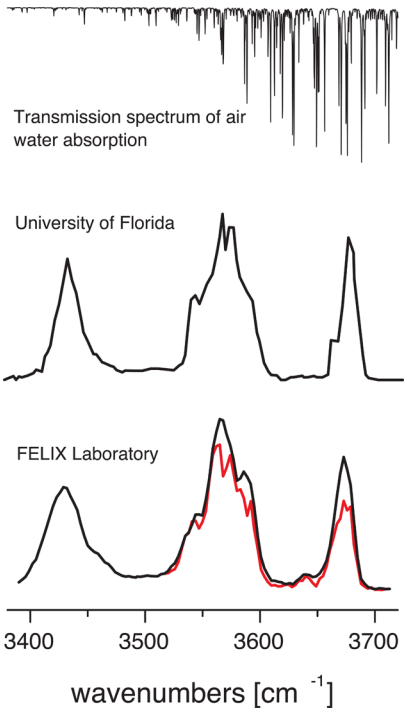

Figure 6. Experimental IRMPD spectra of Rb^+-*O*-methyl-α-D-glucopyranoside obtained at the University of Florida and the FELIX Laboratory. The upper panel shows the transmission spectrum of laboratory air measured with an FTIR spectrometer. The red spectrum in the lower trace was obtained with a reduced dry nitrogen purge in the infrared beamline (see text for details).

DOI: 10.1021/acs.jpcb.5b06563
J. Phys. Chem. B 2015, 119, 12970−12981

spectra obtained with two different FTICR instruments and two different OPO lasers. The "notch" in the UF spectrum at ~3570 cm^{-1} is exactly at the wavenumber value of a strong water absorption band. Although the UF OPO system and laser beam path into the FTICR mass spectrometer were continually purged with dry N_2 gas, removal of water vapor was not complete, as can be seen by comparing the IRMPD spectrum with the IR transmission spectrum of laboratory air, which is shown in the top panel of Figure 6. The FELIX Laboratory spectrum was obtained after extensive and apparently successful purging of the entire laser beam path, until the notch is no longer seen. A slight reduction of the nitrogen purging led to "dips" in the IRMPD spectrum as a result of absorption of IR laser light by water vapor in the path of the laser prior to entering the FTICR instrument (see red spectrum in Figure 6). The extensive purging shows that the shoulders seen in both spectra at ~3540 and 3580 cm^{-1} are real bands which can be attributed to the O−H stretching bands of low-energy coordination conformers, as is suggested by the theoretically predicted bands seen in Figure 2.

CONCLUSIONS

Variable-wavelength multiple-photon dissociation of methyl-glycoside-rubidium adducts using an OPO laser in the C−H and O−H stretch regions yields gas-phase action spectra of high resolution that readily differentiate their stereochemistries. Density functional theory calculations indicate that more than one positional coordination isomer or conformer contribute to the overall spectrum and that these may be bi- or tridentate coordination complexes with rubidium associated with oxygen lone pairs. Measurements made on two separate instruments at two facilities indicate that the spectra are reproducible and that the O−H stretch region, in particular, may be highly advantageous in providing unique spectral fingerprints in the gas phase for sugars having defined stereochemistries.

ASSOCIATED CONTENT

Supporting Information

The Supporting Information is available free of charge on the ACS Publications website at DOI: 10.1021/acs.jpcb.5b06563.

Figures SI-1 and SI-2; complete listing of authors for ref 71 (PDF)

AUTHOR INFORMATION

Corresponding Author

*E-mail: eylerjr@chem.ufl.edu.

Present Addresses

†(W.L.P.) Department of Physics, J.R. Macdonald Laboratory, Kansas State University, Manhattan, Kansas 66506, United States.

‡(C.C.) NASA Ames Research Center, Moffett Field, California 94035, United States.

Notes

The authors declare no competing financial interest.

ACKNOWLEDGMENTS

We thank Nicolas Polfer for many helpful discussions and Nicole Horenstein for assistance with theoretical calculations. Work at UF was supported in part by the U.S. National Science Foundation under CHE-0718007 and INT-0730072. Work at the FELIX Laboratory is part of the research program of FOM, which is financially sponsored by The Netherlands Organization for Scientific Research (NWO).

REFERENCES

(1) Nelson, D. L.; Cox, M. M. *Lehninger Principles of Biochemistry*, 6th ed.; W.H. Freeman: New York, 2012.

(2) Rao, V. S. R.; Qasba, P. K.; Balaji, P. V.; Chandrasekaran, R. *Conformation of Carbohydrates*; Overseas Publishers Association N.V.: Amsterdam, 1998.

(3) Isbell, H. S. *Carbohydrates in Solution*; American Chemical Society: Washington, DC, 1973; Vol. *117*.

(4) Harvey, D. J. Matrix-Assisted Laser Desorption/Ionization Mass Spectrometry of Carbohydrates. *Mass Spectrom. Rev.* **1999**, *18*, 349−450.

(5) Schalley, C. A. Molecular Recognition and Supramolecular Chemistry in the Gas Phase. *Mass Spectrom. Rev.* **2001**, *20*, 253−309.

(6) Zaia, J. Mass Spectrometry of Oligosaccharides. *Mass Spectrom. Rev.* **2004**, *23*, 161−227.

(7) Dole, M.; Mack, L. L.; Hines, R. L.; Mobley, R. C.; Ferguson, L. D.; Alice, M. B. Molecular Beams of Macroions. *J. Chem. Phys.* **1968**, *49*, 2240−2249.

(8) Tanaka, K.; Ido, Y.; Akita, S.; Yoshida, Y.; Yoshida, T. Detection of High Mass Molecules by Laser Desorption Mass Spectrometry. *Iyo Masu Kenkyukai Koenshu* **1987**, *12*, 219−222.

(9) Karas, M.; Hillenkamp, F. Laser Desorption Ionization of Proteins with Molecular Masses Exceeding 10000 Da. *Anal. Chem.* **1988**, *60*, 2299−2301.

(10) Fenn, J. B.; Mann, M.; Meng, C. K.; Wong, S. F.; Whitehouse, C. M. Electrospray Ionization for Mass-Spectrometry of Large Biomolecules. *Science* **1989**, *246*, 64−71.

(11) van den Boom, D.; Hillenkamp, F. Analysis of Nucleic Acids by Mass Spectrometry. *Anal. Technol. DNA Sequencing* **2005**, 85−105.

(12) *Electrospray and Maldi Mass Spectrometry: Fundamentals, Instrumentation, Practicalities, and Biological Applications*, 2nd ed.; Cole, R. B., Ed.; John Wiley and Sons: Hoboken, NJ, 2010.

(13) Marshall, A. G.; Grosshans, P. B. Fourier-Transform Ion-Cyclotron Resonance Mass-Spectrometry - the Teenage Years. *Anal. Chem.* **1991**, *63*, 215A−229A.

(14) Amster, I. J. Fourier Transform Mass Spectrometry. *J. Mass Spectrom.* **1996**, *31*, 1325−1337.

(15) Marshall, A. G.; Hendrickson, C. L.; Jackson, G. S. Fourier Transform Ion Cyclotron Resonance Mass Spectrometry: A Primer. *Mass Spectrom. Rev.* **1998**, *17*, 1−35.

(16) Park, Y.; Lebrilla, C. B. Application of Fourier Transform Ion Cyclotron Resonance Mass Spectrometry to Oligosaccharides. *Mass Spectrom. Rev.* **2005**, *24*, 232−264.

(17) Marshall, A. G.; Hendrickson, C. L.; Emmett, M. R.; Rodgers, R. P.; Blakney, G. T.; Nilsson, C. L. Fourier Transform Ion Cyclotron Resonance: State of the Art. *Eur. Mass Spectrom.* **2007**, *13*, 57−59.

(18) Smith, R. D.; Loo, J. A.; Edmonds, C. G.; Barinaga, C. J.; Udseth, H. R. New Developments in Biochemical Mass Spectrometry: Electrospray Ionization. *Anal. Chem.* **1990**, *62*, 882−899.

(19) Mann, M.; Wilm, M. Electrospray Mass Spectrometry for Protein Characterization. *Trends Biochem. Sci.* **1995**, *20*, 219−224.

(20) Boyd, R.; Brodbelt, J. Electrospray Ionization Mass Spectrometry: Fundamentals, Instrumentation, and Applications. *J. Am. Soc. Mass Spectrom.* **1997**, *8*, 1191−1194.

(21) Busch, K. L.; Glish, G. L.; McLuckey, S. A. *Mass Spectrometry/Mass Spectrometry: Techniques and Applications of Tandem Mass Spectrometry*; VCH Verlagsgesellschaft: Weinheim, Basel, Cambridge, NY, 1988.

(22) Hofmeister, G. E.; Zhou, Z.; Leary, J. A. Linkage Position Determination in Lithium-Cationized Disaccharides - Tandem Mass-Spectrometry and Semiempirical Calculations. *J. Am. Chem. Soc.* **1991**, *113*, 5964−5970.

(23) Fura, A.; Leary, J. A. Differentiation of Ca^{2+}-Coordinated and Mg^{2+}-Coordinated Branched Trisaccharide Isomers - an Electrospray-Ionization and Tandem Mass-Spectrometry Study. *Anal. Chem.* **1993**, *65*, 2805−2811.

DOI: 10.1021/acs.jpcb.5b06563
J. Phys. Chem. B 2015, 119, 12970−12981

(24) Konig, S.; Leary, J. A. Evidence for Linkage Position Determination in Cobalt Coordinated Pentasaccharides Using Ion Trap Mass Spectrometry. *J. Am. Soc. Mass Spectrom.* **1998**, *9*, 1125−1134.
(25) Salpin, J. Y.; Tortajada, J. Structural Characterization of Hexoses and Pentoses Using Lead Cationization. An Electrospray Ionization and Tandem Mass Spectrometric Study. *J. Mass Spectrom.* **2002**, *37*, 379−388.
(26) Jiang, Y. J.; Cole, R. B. Oligosaccharide Analysis Using Anion Attachment in Negative Mode Electrospray Mass Spectrometry. *J. Am. Soc. Mass Spectrom.* **2005**, *16*, 60−70.
(27) Fang, T. T.; Bendiak, B. The Stereochemical Dependence of Unimolecular Dissociation of Monosaccharide-Glycolaldehyde Anions in the Gas Phase: A Basis for Assignment of the Stereochemistry and Anomeric Configuration of Monosaccharides in Oligosaccharides by Mass Spectrometry Via a Key Discriminatory Product Ion of Disaccharide Fragmentation, M/Z 221. *J. Am. Chem. Soc.* **2007**, *129*, 9721−9736.
(28) Rodrigues, J. A.; Taylor, A. M.; Sumpton, D. P.; Reynolds, J. C.; Pickford, R.; Thomas-Oates, J. Mass Spectrometry of Carbohydrates: Newer Aspects. *Adv. Carbohydr. Chem. Biochem.* **2008**, *61*, 59−141.
(29) Bendiak, B.; Fang, T. T. Assignment of the Stereochemistry and Anomeric Configuration of Structurally Informative Product Ions Derived from Disaccharides: Infrared Photodissociation of Glycosyl-Glycolaldehydes in the Negative Ion Mode. *Carbohydr. Res.* **2010**, *345*, 2390−2400.
(30) Eyler, J. R. Infrared Multiple Photon Dissociation Spectroscopy of Ions in Penning Traps. *Mass Spectrom. Rev.* **2009**, *28*, 448−467.
(31) Polfer, N. C.; Oomens, J. Vibrational Spectroscopy of Bare and Solvated Ionic Complexes of Biological Relevance. *Mass Spectrom. Rev.* **2009**, *28*, 468−494.
(32) Fridgen, T. D. Infrared Consequence Spectroscopy of Gaseous Protonated and Metal Ion Cationized Complexes. *Mass Spectrom. Rev.* **2009**, *28*, 586−607.
(33) Valle, J. J. *Differentiation of Carbohydrate Stereoisomers by Infrared Multiple Photon Dissociation Spectroscopy Using a Free Electron Laser and a Fourier Transform Ion Cyclotron Resonance Mass Spectrometer*; University of Florida: Gainesville, FL, 2005. Copyright 2005, Jose J. Valle. All Rights Reserved.
(34) Valle, J. J.; Eyler, J. R.; Oomens, J.; Moore, D. T.; van der Meer, A. F. G.; von Helden, G.; Meijer, G.; Hendrickson, C. L.; Marshall, A. G.; Blakney, G. T. Free Electron Laser-Fourier Transform Ion Cyclotron Resonance Mass Spectrometry Facility for Obtaining Infrared Multiphoton Dissociation Spectra of Gaseous Ions. *Rev. Sci. Instrum.* **2005**, *76*, 023103−7.
(35) Polfer, N. C.; Valle, J. J.; Moore, D. T.; Oomens, J.; Eyler, J. R.; Bendiak, B. Differentiation of Isomers by Wavelength-Tunable Infrared Multiple-Photon Dissociation-Mass Spectrometry: Application to Glucose-Containing Disaccharides. *Anal. Chem.* **2006**, *78*, 670−679.
(36) Stefan, S. E.; Eyler, J. R. Differentiation of Methyl-Glucopyranoside Anomers by Infrared Multiple Photon Dissociation with a Tunable CO_2 Laser. *Anal. Chem.* **2009**, *81*, 1224−1227.
(37) Stefan, S. E.; Eyler, J. R. Differentiation of Glucose-Containing Disaccharides by Infrared Multiple Photon Dissociation with a Tunable CO_2 Laser and Fourier Transform Ion Cyclotron Resonance Mass Spectrometry. *Int. J. Mass Spectrom.* **2010**, *297*, 96−101.
(38) Cagmat, E. B.; Szczepanski, J.; Pearson, W. L.; Powell, D. H.; Eyler, J. R.; Polfer, N. C. Vibrational Signatures of Metal-Chelated Monosaccharide Epimers: Gas-Phase Infrared Spectroscopy of Rb^+-Tagged Glucuronic and Iduronic Acid. *Phys. Chem. Chem. Phys.* **2010**, *12*, 3474−3479.
(39) Stefan, S. E.; Ehsan, M.; Pearson, W. L.; Aksenov, A.; Boginski, V.; Bendiak, B.; Eyler, J. R. Differentiation of Closely Related Isomers: Application of Data Mining Techniques in Conjunction with Variable Wavelength Infrared Multiple Photon Dissociation Mass Spectrometry for Identification of Glucose-Containing Disaccharide Ions. *Anal. Chem.* **2011**, *83*, 8468−8476.
(40) Brown, D. J.; Stefan, S. E.; Berden, G.; Steill, J. D.; Oomens, J.; Eyler, J. R.; Bendiak, B. Direct Evidence for the Ring Opening of Monosaccharide Anions in the Gas Phase: Photodissociation of Aldohexoses and Aldohexoses Derived from Disaccharides Using Variable-Wavelength Infrared Irradiation in the Carbonyl Stretch Region. *Carbohydr. Res.* **2011**, *346*, 2469−2481.
(41) Schindler, B.; Joshi, J.; Allouche, A.-R.; Simon, D.; Chambert, S.; Brites, V.; Gaigeot, M.-P.; Compagnon, I. Distinguishing Isobaric Phosphated and Sulfated Carbohydrates by Coupling of Mass Spectrometry with Gas Phase Vibrational Spectroscopy. *Phys. Chem. Chem. Phys.* **2014**, *16*, 22131−22138.
(42) Simons, J. P.; Jockusch, R. A.; Carcabal, P.; Hunig, I.; Kroemer, R. T.; Macleod, N. A.; Snoek, L. C. Sugars in the Gas Phase. Spectroscopy, Conformation, Hydration, Co-Operativity and Selectivity. *Int. Rev. Phys. Chem.* **2005**, *24*, 489−531.
(43) Alonso, J. L.; Lozoya, M. A.; Pena, I.; Lopez, J. C.; Cabezas, C.; Mata, S.; Blanco, S. The Conformational Behaviour of Free D-Glucose-at Last. *Chem. Sci.* **2014**, *5*, 515−522.
(44) Cocinero, E. J.; Lesarri, A.; Ecija, P.; Basterretxea, F. J.; Grabow, J.-U.; Fernandez, J. A.; Castano, F. Ribose Found in the Gas Phase. *Angew. Chem., Int. Ed.* **2012**, *51*, 3119−3124.
(45) Franks, F.; Hall, J. R.; Irish, D. E.; Norris, K. The Effect of Cations on the Anomeric Equilibrium of D-Glucose in Aqueous Solutions - a Raman-Spectral Study. *Carbohydr. Res.* **1986**, *157*, 53−64.
(46) Angyal, S. J. Complexes of Metal Cations with Carbohydrates in Solution. *Adv. Carbohydr. Chem. Biochem.* **1989**, *47*, 1−43.
(47) Dais, P. Carbon-13 Nuclear Magnetic Relaxation and Motional Behavior of Carbohydrate Molecules in Solution. *Adv. Carbohydr. Chem. Biochem.* **1995**, *51*, 63−131.
(48) Gessler, K.; Krauss, N.; Steiner, T.; Betzel, C.; Sarko, A.; Saenger, W. β-D-Cellotetraose Hemihydrate as a Structural Model for Cellulose II. An X-Ray Diffraction Study. *J. Am. Chem. Soc.* **1995**, *117*, 11397−406.
(49) Jeffrey, G. A.; Sundaralingam, M. Bibliography of Crystal Structures of Carbohydrates, Nucleosides, and Nucleotides for 1979 and 1980; Addenda and Errata from 1970−1978; and Index for 1935−1980. *Adv. Carbohydr. Chem. Biochem.* **1985**, *43*, 203−421.
(50) Honda, S.; Yamamoto, K.; Suzuki, S.; Ueda, M.; Kakehi, K. High-Performance Capillary Zone Electrophoresis of Carbohydrates in the Presence of Alkaline Earth Metal Ions. *J. Chromatogr.* **1991**, *588*, 327−233.
(51) Honda, S. Separation of Neutral Carbohydrates by Capillary Electrophoresis. *J. Chromatogr., A* **1996**, *720*, 337−351.
(52) Cerda, B. A.; Wesdemiotis, C. Thermochemistry and Structures of Na^+ Coordinated Mono- and Disaccharide Stereoisomers. *Int. J. Mass Spectrom.* **1999**, *189*, 189−204.
(53) Perez, S. Molecular Modeling in Glycoscience. In *Comprehensive Glycoscience—From Chemistry to Systems Biology*; Kamerling, J. P., Ed.; Elsevier: Amsterdam, 2007; Vol. 2, pp 347−388.
(54) Varki, A. Glycan-Based Interactions Involving Vertebrate Sialic-Acid-Recognizing Proteins. *Nature* **2007**, *446*, 1023−1029.
(55) Kajihara, Y.; Tanabe, Y.; Sasaoka, S.; Okamoto, R. Homogeneous Human Complex-Type Oligosaccharides in Correctly Folded Intact Glycoproteins: Evaluation of Oligosaccharide Influence on Protein Folding, Stability, and Conformational Properties. *Chem. - Eur. J.* **2012**, *18*, 5944−5953.
(56) Zhou, Z.; Ogden, S.; Leary, J. A. Linkage Position Determination in Oligosaccharides: Mass Spectrometry (MS/MS) Study of Lithium-Cationized Carbohydrates. *J. Org. Chem.* **1990**, *55*, 5444−5446.
(57) Polfer, N. C.; Oomens, J.; Moore, D. T.; von Helden, G.; Meijer, G.; Dunbar, R. C. Infrared Spectroscopy of Phenylalanine Ag(I) and Zn(II) Complexes in the Gas Phase. *J. Am. Chem. Soc.* **2006**, *128*, 517−525.
(58) Polfer, N. C.; Oomens, J. Reaction Products in Mass Spectrometry Elucidated with Infrared Spectroscopy. *Phys. Chem. Chem. Phys.* **2007**, *9*, 3804−3817.

DOI: 10.1021/acs.jpcb.5b06563
J. Phys. Chem. B 2015, 119, 12970−12981

(59) Marshall, A. G.; Wang, T. C. L.; Ricca, T. L. Tailored Excitation for Fourier-Transform Ion-Cyclotron Resonance Mass-Spectrometry. *J. Am. Chem. Soc.* **1985**, *107*, 7893−7897.
(60) Guan, S. H.; Marshall, A. G. Stored Waveform Inverse Fourier Transform (SWIFT) Ion Excitation in Trapped-Ion Mass Spectometry: Theory and Applications. *Int. J. Mass Spectrom. Ion Processes* **1996**, *157-158*, 5−37.
(61) Strossner, U.; Meyn, J.-P.; Wallenstein, R.; Urenski, P.; Arie, A.; Rosenman, G.; Mlynek, J.; Schiller, S.; Peters, A. Single-Frequency Continuous-Wave Optical Parametric Oscillator System with an Ultrawide Tuning Range of 550 to 2830 nm. *J. Opt. Soc. Am. B* **2002**, *19*, 1419−1424.
(62) van Herpen, M. M. J. W.; Bisson, S. E.; Ngai, A. K. Y.; Harren, F. J. M. Combined Wide Pump Tuning and High Power of a Continuous-Wave, Singly Resonant Optical Parametric Oscillator. *Appl. Phys. B: Lasers Opt.* **2004**, *78*, 281−286.
(63) Oh, H.; Breuker, K.; Sze, S. K.; Ge, Y.; Carpenter, B. K.; McLafferty, F. W. Secondary and Tertiary Structures of Gaseous Protein Ions Characterized by Electron Capture Dissociation Mass Spectrometry and Photofragment Spectroscopy. *Proc. Natl. Acad. Sci. U. S. A.* **2002**, *99*, 15863−15868.
(64) Oh, H.-B.; Lin, C.; Hwang, H. Y.; Zhai, H.; Breuker, K.; Zabrouskov, V.; Carpenter, B. K.; McLafferty, F. W. Infrared Photodissociation Spectroscopy of Electrosprayed Ions in a Fourier Transform Mass Spectrometer. *J. Am. Chem. Soc.* **2005**, *127*, 4076−4083.
(65) Bush, M. F.; O'Brien, J. T.; Prell, J. S.; Wu, C.-C.; Saykally, R. J.; Williams, E. R. Hydration of Alkaline Earth Metal Dications: Effects of Metal Ion Size Determined Using Infrared Action Spectroscopy. *J. Am. Chem. Soc.* **2009**, *131*, 13270−13277.
(66) O'Brien, J. T.; Williams, E. R. Effects of Ions on Hydrogen-Bonding Water Networks in Large Aqueous Nanodrops. *J. Am. Chem. Soc.* **2012**, *134*, 10228−10236.
(67) Moghaddam, M. B.; Fridgen, T. D. IRMPD Spectroscopic Study of Microsolvated $[Na(GlyAla)]^+$ and $[Ca(GlyAla-H)]^+$ and the Blue Shifting of the Hydrogen-Bonded Amide Stretch with Each Water Addition. *J. Phys. Chem. B* **2013**, *117*, 6157−6164.
(68) Almasian, M.; Grzetic, J.; van Maurik, M. J.; Steill, J. D.; Berden, G.; Ingemann, S.; Buma, W. J.; Oomens, J. Non-Equilibrium Isomer Distribution of the Gas-Phase Photoactive Yellow Protein Chromophore. *J. Phys. Chem. Lett.* **2012**, *3*, 2259−2263.
(69) Heine, N.; Fagiani, M. R.; Rossi, M.; Wende, T.; Berden, G.; Blum, V.; Asmis, K. R. Isomer-Selective Detection of Hydrogen-Bond Vibrations in the Protonated Water Hexamer. *J. Am. Chem. Soc.* **2013**, *135*, 8266−8273.
(70) Ung, H. U.; Moehlig, A. R.; Khodagholian, S.; Berden, G.; Oomens, J.; Morton, T. H. Proton-Bridge Motions in Amine Conjugate Acid Ions Having Intramolecular Hydrogen Bonds to Hydroxyl and Amine Groups. *J. Phys. Chem. A* **2013**, *117*, 1360−1369.
(71) Frisch, M. J.; Trucks, G. W.; Schlegel, H. B.; Scuseria, G. E.; Robb, M. A.; Cheeseman, J. R.; Scalmani, G.; Barone, V.; Mennucci, B.; Petersson, G. A., et al. *Gaussian 09*, revision C.01; Gaussian, Inc.: Wallingford CT, 2009.
(72) Allouche, A.-R. Gabedit - a Graphical User Interface for Computational Chemistry Softwares. *J. Comput. Chem.* **2011**, *32*, 174−182.
(73) Contreras, C. S.; Polfer, N. C.; Oomens, J.; Steill, J. D.; Bendiak, B.; Eyler, J. R. On the Path to Glycan Conformer Identification: Gas-Phase Study of the Anomers of Methyl Glycosides of N-Acetyl-D-Glucosamine and N-Acetyl-D-Galactosamine. *Int. J. Mass Spectrom.* **2012**, *330−332*, 285−294.
(74) Tipson, R. S.; Parker, F. S. Infrared Spectroscopy. In *The Carbohydrates, Chemistry and Biochemistry*, 2nd ed.; Pigman, W., Horton, D., Eds.; Academic Press: New York, 1980.
(75) For example, see: Gas-Phase IR Spectroscopy and Structure of Biological Molecules. In *Topics in Current Chemistry 352*; Rijs, A. M., Oomens, J., Eds.; Springer SBM: Dordrecht, The Netherlands, 2015.
(76) Patrick, A. L.; Stedwell, C. N.; Schindler, B.; Compagnon, I.; Berden, G.; Oomens, J.; Polfer, N. C. Insights into the Fragmentation Pathways of Gas-Phase Protonated Sulfoserine. *Int. J. Mass Spectrom.* **2015**, *379*, 26−32.
(77) Hernandez, O.; Paizs, B.; Maitre, P. Rearrangement Chemistry of Ions Probed by IR Spectroscopy. *Int. J. Mass Spectrom.* **2015**, *377*, 172−178.

DOI: 10.1021/acs.jpcb.5b06563
J. Phys. Chem. B 2015, 119, 12970−12981